FUNDAMENTALS & APPLICATIONS

CHEMELECTROCHEM

ANALYSIS & CATALYSIS, BIO & NANO, ENERGY & MORE

Accepted Article

Title: Hematite Nanorod Electrodes Modified with Molybdenum: Photoelectrochemical Studies

Authors: Ainhoa Cots, Dejan Cibrev, Pedro Bonete, and Roberto Gómez

To be cited as: *ChemElectroChem* 10.1002/celc.201600644

Link to VoR: http://dx.doi.org/10.1002/celc.201600644

A Journal of

ChemPubSoc Europe

WILEY-VCH

www.chemelectrochem.org

ARTICLE WILEY-VCH

Hematite Nanorod Electrodes Modified with Molybdenum: Photoelectrochemical Studies.

Ainhoa Cots[a], Dejan Cibrev[a], Pedro Bonete[a], Roberto Gómez*[a]

Abstract: The preparation of hematite nanorod electrodes modified with molybdenum and their photoelectrochemical behavior for water photooxidation have been addressed in the quest for improved electrodes for water splitting. The hematite nanorods were synthesized by chemical bath deposition, while Mo was added by following two variants of a drop casting method based on ammonium heptamolybdate solutions. FE-SEM, TEM, XRD and XPS were employed for electrode structural and morphological characterization. The reported results reveal that the impregnation method does not cause significant changes in the hematite structure and nanorod morphology. Importantly, the modification with Mo triggers a significant improvement in the photoactivity of the electrodes, obtaining a photocurrent increase of up to 43x. A specific Mott-Schottky analysis applicable to nanostructured electrodes was performed, revealing that the modification with Mo leads to an increase in electron concentration and to a shift of the flat band potential toward more positive values. A second role of Mo as a passivating agent needs to be invoked to explain the experimental observations. It is worth noting that this modification method allows a precise control of the amount of Mo contained in the samples while maintaining the morphology of the electrode.

Introduction

The increasing global energy demand and the emission of pollutant gases to the atmosphere due to the use of fossil fuels require further research in environmentally friendly alternatives. In this respect, hydrogen gas is a carbon-free fuel with a high energy density. Inspired by natural photosynthesis, artificial photosynthesis has captured a lot of attention as a way to obtain hydrogen in a clean and renewable way. In this context, photoelectrochemical water splitting based on semiconductors potentially represents a green and low cost method to generate hydrogen. Although an energy of only about 2 eV is necessary to overcome the thermodynamic and typical kinetic barriers to photoelectrochemical water splitting, a semiconductor material capable of efficiently converting solar energy into hydrogen has not been found yet [1,2]. In any case, the conversion efficiency can be improved through the joint use of two photoelectrodes with complementary light absorption. These devices are known as tandem cells and comprise a photocathode where solar hydrogen generation occurs and a photoanode where water oxidation takes place [3,4].

Since the first demonstration of photoelectrochemical water splitting using TiO_2, a large number of semiconductors have been studied as photoelectrodes, such as ZnO, α-Fe_2O_3, $BiVO_4$, WO_3, SiC, CdS and GaP [1,2,5–10]. According to their chemical nature, band gap positions and electrochemical properties, they can be used as either photoanodes or photocathodes. It is also worth noting the increasing importance of iron-group metal oxides in water splitting and artificial photosynthesis.[11,12] In fact, among the many metal oxides suggested as candidates for photoelectrochemical water splitting some characteristics of hematite such as its abundance, stability low cost and favorable band gap, suggest that it could be a promising photoanode [13–15]. In recent years several studies have shown the potential of hematite photoelectrodes, although the use of this material as a photoanode is limited by its high recombination rate, low carrier mobility, slow carrier transfer and relatively weak light absorption [13,16–21]. These limitations imply that different modification strategies need to be applied before hematite can be used in practice.

Extensive efforts have been directed toward modifying α-Fe_2O_3 electrodes to improve their photoconversion. Nowadays, a variety of rational strategies has been developed to overcome hematite limitations for efficient water splitting, for instance i) reducing bulk recombination by developing nanostructured architectures, ii) improving conductivity, iii) promoting charge transfer ability by metal ion doping, and iv) improving water oxidation kinetics using catalysts [13,22,23]. A substantial part of the reported improvements in photocurrent density can be attributed to advances in nanostructure design and metal ion doping, which facilitate charge transport and, thus, allows for efficient charge collection. A synergetic effect in the combination of nanostructured design and ion doping was observed for example with Ti-doped hematite nanostructures [22,24]. Focusing on doping, Mo, Cr, Si, Ti, Zr, Ta, Nb, Bi, Ge, Mn, and especially Sn, are some of the dopants described in the literature [13,14,25–38]. There are a number of methods that can be used for doping hematite electrodes. The most common ones are methods based on impregnation (such as drop casting), electrodeposition, and hydrothermal treatment. Among them, there are a few studies dealing with molybdenum as a dopant, standing out the theoretical work published by Qin *et al*. [39] and the experimental results reported by McFarland *et al*.[25]. In the first case, the authors indicated that the photoelectrochemical efficiency of hematite as a photoanode should increase upon Mo doping due to a combination of a reduced band gap and an increased carrier concentration. On the other hand, McFarland *et al.* demonstrated a substantial enhancement of the hematite

[a] A. Cots; D. Cibrev, Dr. P. Bonete, Dr. R. Gómez
Departament de Química Física i Institut Universitari d'Electroquímica
Universitat d'Alacant
Apartat 99, E- 03080 Alicante (Spain)
E-mail: roberto.gomez@ua.es
(*) Corresponding author
Supporting information for this article is given via a link at the end of the document.

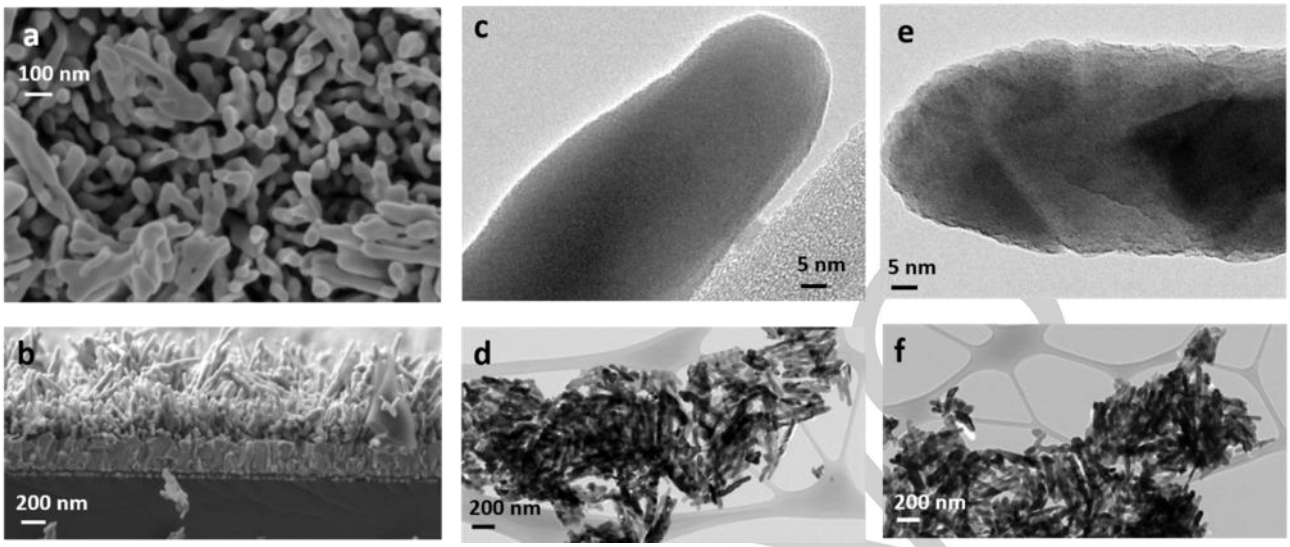

Figure 1. Top-view (a) and cross-section (b) FE-SEM images of pristine hematite nanostructured films; TEM images for pristine hematite (c and d) and Mo-modified hematite (Mo_6) (e and f).

photoanode performance upon introduction of molybdenum through electrochemical co-deposition.

In this work, a simple and novel strategy for improving the water photooxidation capability of hematite nanorod electrodes has been studied using molybdenum as a dopant. The hematite electrodes have been modified by means of drop casting with ammonium heptamolybdate solutions. Several techniques such as SEM, TEM, XRD, and XPS have been employed to carry out the physical characterization of the different electrodes. Subsequent photoelectrochemical characterization evinces the improvement in photoactivity caused by modification with molybdenum.

Results and Discussion

All the results reported below correspond to several (4) series of experiments. The most representative behavior is shown in each case.

Sample characterization

Figure 1 shows the FE-SEM (Figure 1a-b) and TEM images (Figure 1c-f) for both pristine and Mo-modified hematite samples. As observed from FE-SEM images, the hematite films are composed, as expected, of oriented nanorods. The cross-section of the FTO-hematite electrode shows that the thickness of the hematite film is approximately equal to 400 nm. The FE-SEM images corresponding to the modification of hematite by the addition of Mo by drop casting are not presented as they are virtually identical to those shown in Figure 1a-b. The TEM images (Figure 1c-f) for both pristine and Mo-modified hematite samples are given at two different magnifications. As shown in Figure 1e, the addition of Mo by drop casting leads to an increase in roughness of the nanorod walls compared to pristine hematite (Figure 1c), which could be linked to the formation of a Mo-rich surface layer, although the morphology (aspect ratio) of the nanorods does not significantly change. Additional SEM and TEM images for samples with a higher Mo loading (Figure S1) do not show signs of the formation of agglomerates, being the morphology of the nanorods preserved.

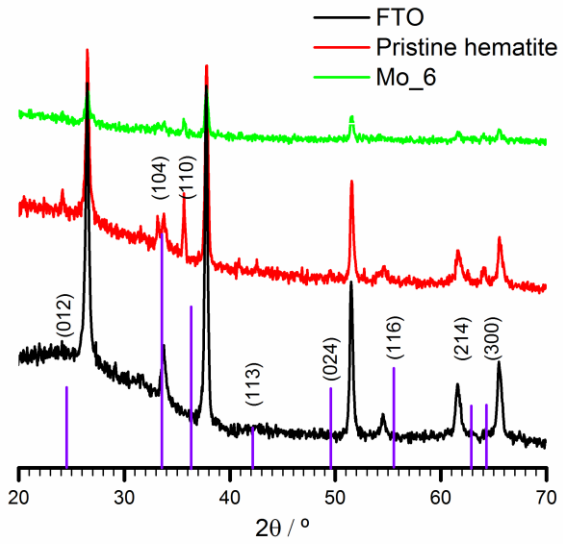

Figure 2. X-Ray diffractograms for pristine hematite, Mo-modified hematite (Mo_6) and FTO. Hematite main peaks are shown in purple and are labeled.

X-ray diffractograms (XRD) for different electrodes are shown in Figure 2. The diffractograms confirm the existence of predominantly (110) oriented hematite (α-Fe_2O_3) for both pristine and Mo-modified samples although there is some dispersion in the orientation. The unlabeled peaks correspond to SnO_2 (casiterite phase) from the conducting glass substrate. The observed hematite peaks were identified using the JCPDS

catalog as a reference for standard values. Therefore, Mo-modification does not trigger a change of the hematite structure.

Figure 3 shows the XPS spectra for the Fe 2p and Mo 3d regions for the different samples. The Fe 2p spectra (Figure 3a) are rather similar in both cases and can be attributed completely to Fe^{3+}. The high resolution Mo 3d XPS spectra are shown in Figure 3b. For hematite modified with Mo by both one-step (Mo_6, 8.1 nmol Mo·cm^{-2}) and multiple-step drop-casting (Mo_S2, 1.62 nmol Mo·cm^{-2}), the Mo $3d_{5/2}$ peak is centered at 232.5 eV, attributed to Mo^{6+}, coinciding with the Mo oxidation state in the precursor solution [25,40,41]. Traces of Mo^{5+} could be present in the case of the Mo_S2 sample. In any case, it is worth noting that a semi-quantitative chemical analysis shows that the surface is enriched with molybdenum. The survey XPS spectra are shown in Figure S2 and demonstrate the absence of molybdenum in the sample of pristine hematite. The incorporation of Mo in the hematite nanostructure has also been confirmed by EDX data obtained in parallel with the TEM images.

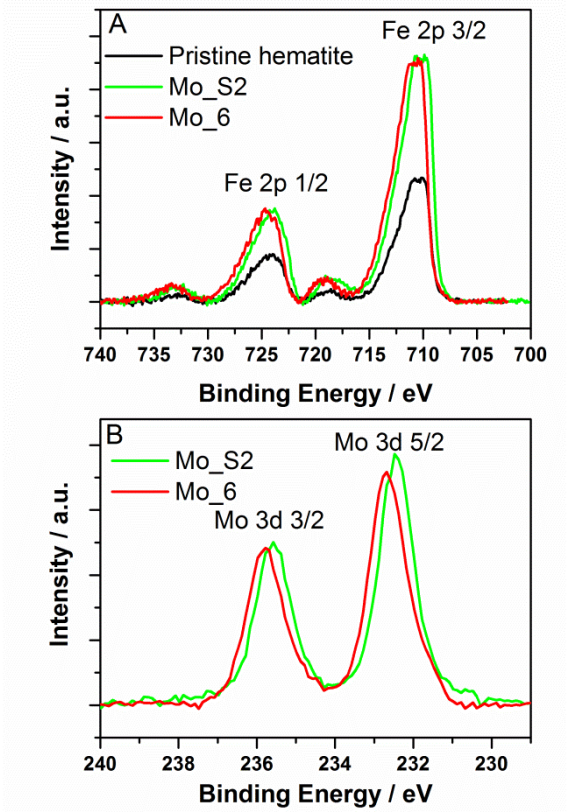

Figure 3. (a) Fe 2p and (b) Mo 3d XPS spectra for pristine, and Mo-modified hematite samples (Mo_6 and Mo_S2).

Finally, Figure 4 shows the UV-vis spectra for both pristine and different Mo-modified hematite electrodes. As observed, the modification with Mo does not trigger significant changes in the absorption spectra of hematite. Therefore, the enhancement observed in the photoactivity of the hematite electrodes upon modification with Mo cannot be attributed to an increased light harvesting ability. The inset of the figure shows the corresponding Tauc plots for the different samples. In all cases, the optical band gap would be of 1.95 eV.

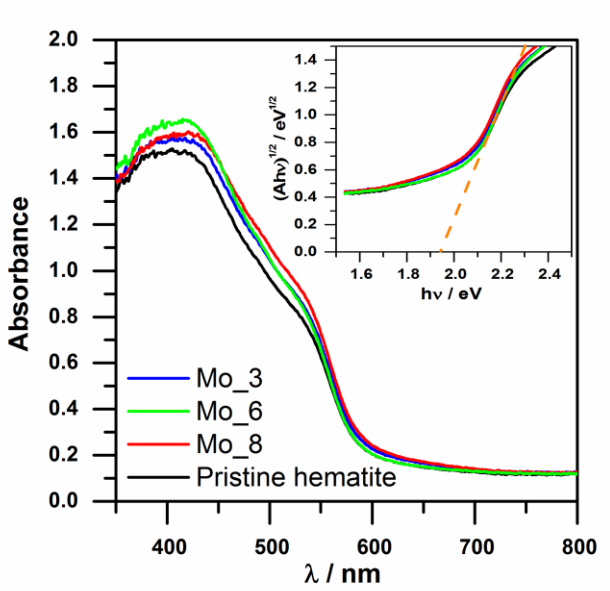

Figure 4. UV-vis spectra for different hematite electrodes both pristine and Mo-modified. Inset: corresponding Tauc plots for an indirect transition semiconductor.

(Photo)electrochemical characterization

The (photo)electrochemical behavior of both pristine and Mo-modified α-Fe_2O_3 samples was studied by means of cyclic voltammetry in the dark and linear voltammetry under illumination. Figure 5 shows voltammograms for both pristine hematite and hematite modified by one-step drop-casting with different amounts of Mo.

Focusing on the voltammograms obtained in the dark (Figure 5a), pristine hematite shows capacitive currents for potentials below -0.2 V, which can be attributed to an accumulation region linked to either conduction band or surface states. The region at potentials positive to 0.4V shows the development of a pseudocapacitive contribution that also contains a faradaic signal associated with the generation of oxygen. This pseudocapacitance is probably linked to the oxidation/reduction of surface Fe (III)/Fe (IV). After the addition of Mo, the electrode capacitance in the accumulation region increases and starts at more positive potentials, while the Mo presence causes the pseudocapacitive signal at potentials positive to 0.4 V to dramatically diminish.

Under illumination (Figure 5b), hematite electrodes show, as expected, anodic photocurrents. Importantly, the addition of different amounts of Mo to the hematite electrode leads to a significant enhancement of the photoresponse, even for Mo loadings of only 0.54 nmol·cm^{-2}. In the optimum case (*Mo*_6, 8.1 nmol Mo·cm^{-2}) a 40-fold increment of the photocurrent is attained. However, it should also be mentioned that, upon the addition of molybdenum, the photo-onset potential slightly shifts to more positive potentials (by less than 50 mV).

Figure 6 shows the dark currents and photocurrents for both pristine and hematite samples modified with Mo by multiple-step drop-casting (0.54 nmol Mo·cm^{-2} per step). As in the case of Mo added in a single step, Figure 6a reveals a strong increase in the capacitive currents in the accumulation region after the addition of Mo. In the same way, Figure 6b shows an increase in the photocurrent for water oxidation peaking at Mo_S2 (28-fold photocurrent increase at 0.23 V). Regarding the photo-onset potential, there is a shift to more positive values, as in the previous case.

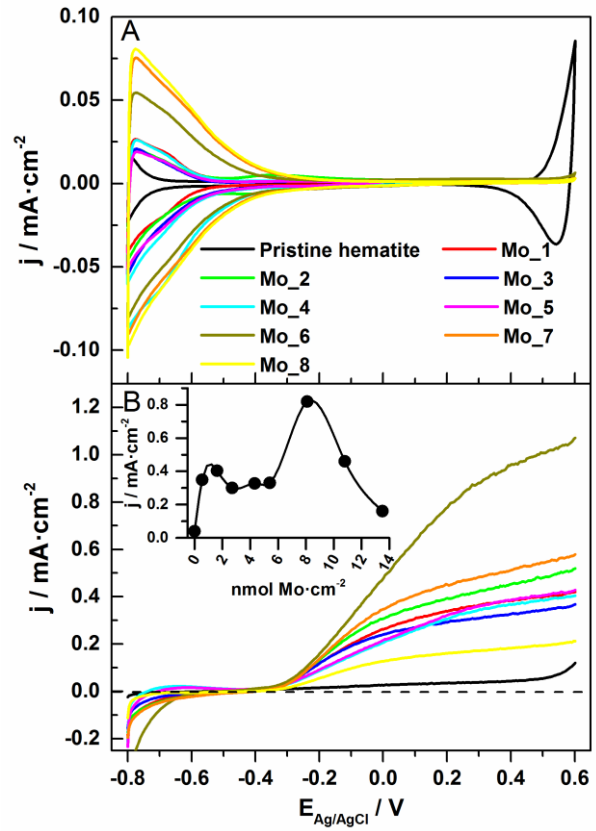

Figure 5. Current density vs potential measured in aqueous N_2-purged 1M NaOH for different modified and pristine hematite electrodes. (a) Cyclic voltammograms obtained in the dark and (b) linear voltammograms obtained under illumination (350 mW·cm^{-2}, λ>350nm) for hematite modified with different amounts of molybdenum dosed by one-step drop casting. Inset shows the photocurrent densities obtained at 0.23 V for the different samples studied.

On the other hand, the stability of the Mo-modified hematite electrodes has been checked in a preliminary way by means of chronoamperometric measurements as shown in Figure S4. As observed, the Mo-modified electrodes show a remarkable short-term stability regardless of both the Mo loading and the drop casting procedure being employed. This is particularly relevant in the case of Mo modification as MoO_3 is soluble in alkaline solutions. As the electrode surface is Mo-enriched, this is an indirect indication that the outermost surface layer is probably constituted by a more stable iron-molydenum oxide, such as ferric molybdate[33].

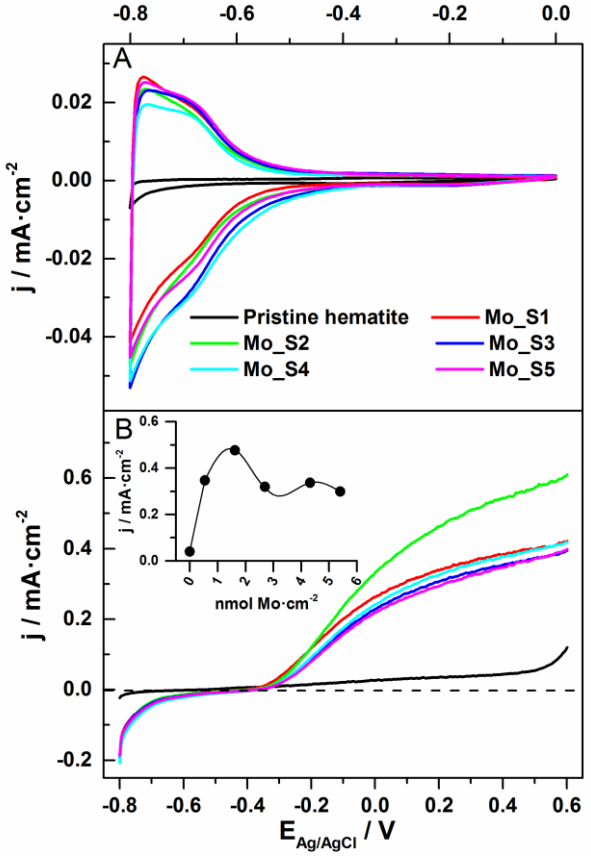

Figure 6. Current density vs potential measured in aqueous N_2-purged 1M NaOH for different modified and pristine hematite electrodes. (a) Cyclic voltammograms obtained in the dark and (b) linear voltammograms obtained under illumination (350 mW·cm^{-2}, λ>350nm) for hematite modified with different amounts of molybdenum dosed by multiple-step drop casting. Inset shows the photocurrent densities obtained at 0.23 V for the different samples studied.

In order to determine the flat band potential and the carrier density for the different electrodes, a Mott-Schottky analysis was performed using a frequency of 1 kHz. It should be borne in mind that the employed electrodes have a 3D morphology, in the sense that the real interfacial area is much larger than the geometric one. As long as the characteristic dimension of the nanoobjects (diameter of nanorods in this case) is larger than that of the space charge region, the Mott-Schottky equation should be written as:

$$\frac{A_{real}^2}{C_{sc}^2} = \frac{2}{e\varepsilon\varepsilon_0 N_d}\left(E - E_{fb} - \frac{kT}{e}\right) \qquad (1)$$

where C_{SC} is the capacitance of the space charge region, A_{real} is the real surface area, which takes into account the electrode roughness, ε_{sc} is the semiconductor dielectric constant, ε_0 is the vacuum permittivity, N_d is the donor density (electron donor concentration for an *n*-type semiconductor), E is the applied potential, and E_{fb} is the flat band potential. If we take into account that the roughness factor (*r*) can be expressed as:

$$r = \frac{A_{real}}{A_{geom}} \qquad (2)$$

where A_{geom} is the geometric (projected) area of the electrode, Equation (1) can be rewritten as:

$$\frac{A_{geom}^2}{C_{sc}^2} = \frac{2}{e\varepsilon\varepsilon_0 N_d r^2}\left(E - E_{fb} - \frac{kT}{e}\right) \qquad (3)$$

Unfortunately, the use of Equation (3) is not widespread. A more detailed discussion on the use of the Mott-Schottky equation for nanostructured electrodes is underway and will be published elsewhere. In the case of a nanorod electrode, the roughness factor can be determined as:

$$r = 1 + 2\pi R h N_{col} \qquad (4)$$

where R is the average nanorod radius, h is the average nanorod height and N_{col} is the average density of nanorod per cm^2. In this case, the roughness factor attains a value of 10.6.

Figure 7 shows Mott-Schottky plots obtained in the dark for pristine hematite and optimum Mo-modified hematite electrodes. The table in the inset gathers the different values obtained for the flat band potential and the carrier density in the dark. To obtain the carrier density, a value of 25 for the hematite dielectric constant was used [42]. The flat band potential for the optimum Mo-modified electrodes shifts toward more positive values by 0.05 V for Mo_S2 and by 0.20 V for Mo_6. The carrier density increases in all cases with respect to pristine hematite, being maximum for hematite modified by adding 8.1 nmol Mo·cm^{-2} (*Mo_6*). The flat band potential was not found to change significantly upon electrode illumination (Figure S5).

Electrochemical impedance spectroscopy (EIS) experiments were done under visible light illumination to study the kinetics of charge transfer processes under PEC operating conditions. Two potentials were chosen: -0.30 V (close to the onset potential) and at 0.23 V (O_2/OH^- equilibrium potential). It is well know that the radius of the semicircles in the frequency range 1-100 Hz corresponds to the charge transfer resistance at the semiconductor/electrolyte interface.[35] As shown in Figure 8, Nyquist plots collected at either -0.30 V or 0.23 V for both pristine and hematite films modified with molybdenum, show that the electrodes modified with Mo have a much smaller impedance arc radius at both potentials, indicating that the charge transfer kinetics is much faster for them. It is remarkable though that the Mo_S2 electrode shows the lowest impedance at -0.3 V (close to the photocurrent onset) while the lowest impedance at 0.23 V is shown by the Mo_6 electrode. The different tendency is linked with the fact that the level of improvement achieved for the different samples is potential-dependent. In this way, for one-step Mo deposition, the improvement was clearer at higher potentials, while in the case of the sequential deposition method, the behavior was preferentially improved at potentials close of the onset (see Figure S3).

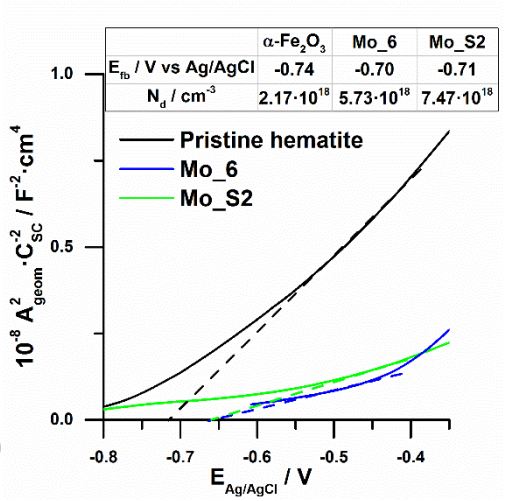

Figure 7. Mott-Schottky plots for α-Fe_2O_3 electrodes either pristine or modified with molybdenum. Data obtained in the dark with a frequency of 1 kHz in N_2-purged aqueous 1M NaOH. The inset table shows the values for the flat-band potential and carrier density for the different electrodes.

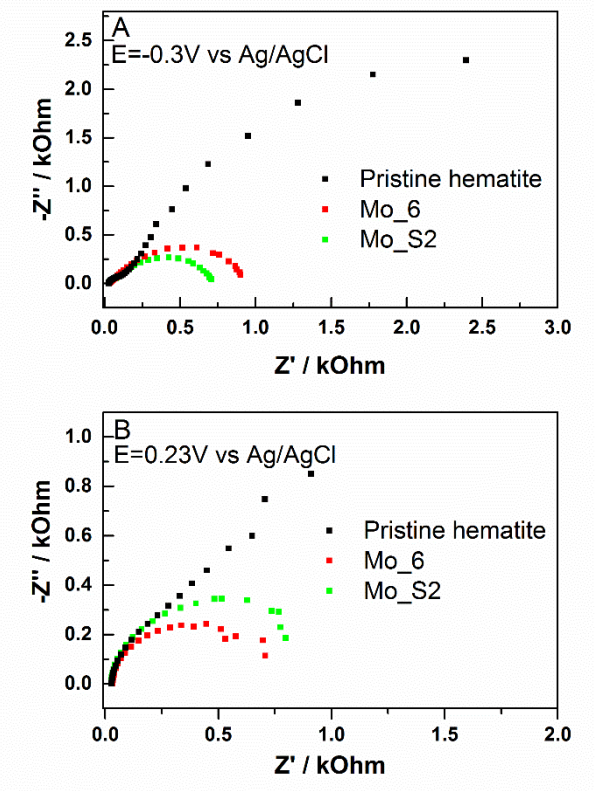

Figure 8. Nyquist plots for pristine and the most-efficient Mo-modified hematite electrodes, (a) at -0.30 V vs. Ag/AgCl and (b) at 0.23 V under illumination conditions (350 mW·cm^{-2}; λ>350 nm) in N_2-purged aqueous 1M NaOH.

Discussion

The UV-vis spectra of the hematite electrodes does not experience significant changes upon Mo modification, which excludes the idea that the photocurrent enhancement may be due to a decrease in band gap and a consequent increase in the light harvesting ability of the material. In any case, the modification of hematite with Mo seems to have a dual effect. On the one hand, Mo enhances the n-character of hematite. On the other, surface Mo species seem to either block surface states or facilitate hole transfer, acting as redox catalytic centers. The first role is revealed by the changes that occur in the electrochemical response of the modified electrodes in the dark. In this respect, the region of charge accumulation at negative potentials increases upon modification with Mo. The capacitance enhancement is mainly attributed to an increase in the conductivity of the hematite thin film. A more direct piece of evidence comes from Mott-Schottky plots, which indicate a significant increase in the concentration of conduction band electrons upon Mo modification. On the other hand, and as deduced from SEM and TEM (Figure 1c and e), the introduction of Mo does not trigger significant morphological changes, although there is an increase in the roughness due to a suface layer of Mo. Thus, it cannot be excluded that the increase in the accumulation region could also be linked to some extent to an enhanced electrochemically active interfacial area. In addition to the Mo-induced surface roughness, there are other indications that a significant amount of Mo remains at the surface of the hematite rods: (i) the voltammetric response in the dark shows that the contribution at potentials higher than 0.4V, partly associated with the oxidation/reduction of Fe(III)/Fe(IV), is completely blocked, and (ii) an XPS analysis points to an enrichment of Mo at the electrode surface. These surface Mo species are expected to alter the ability of the electrode as a photoanode for water splitting by either passivating surface states or by acting as co-catalytic centers. However, the blockage of the voltammetric signals associated with the surface Fe(IV)/Fe(III) redox couple suggests that the passivating effect could be more important. In this respect, it is known that the upper part of the hematite valence band possesses an important contribution of Fe 3d orbitals [13] and therefore a hole trapped at the surface can be seen as a surface Fe(IV). As the modification with Mo avoids the formation of Fe(IV), hole trapping would be hindered, which would correspond to a passivation of surface states linked to the valence band. In addition, molybdenum does not have redox couples in the potential region above 1.23 V vs. RHE, at least in alkaline media, which precludes its role as a catalytic redox center for oxygen evolution. Finally, it is worth noting that, in this case, surface passivation would not lead to the expected negative shift on the onset potential.

In agreement with the above discussion, both the increase in conductivity and surface passivation are likely responsible for the improvement of the photocurrent upon modification with Mo (Figure 9). However, the photocurrent onset and the flat band potential shift toward more positive values, which is inconvenient for the development of effective photoanodes. It should be noted though that, for an optimized modification of hematite with molybdenum (*Mo_6* electrode), this shift is minor (~ 25 mV), as shown in Figure 9b.

It is interesting to examine the effect of Mo as a function of the Mo loading as shown in the insets of Figures 5 and 6. Both tendency graphs reveal that there is an optimum loading of Mo beyond which the performance decreases. This is not unexpected as overmodification can decrease hematite crystallinity and block the hematite surface with a thick layer of molybdenum-rich oxide, precluding an efficient hole transfer to solution. Interestingly, the performance of electrodes with the same Mo loading prepared by multiple-step drop casting is slightly better than that of those prepared by one-step drop casting. It should be kept in mind that in the multiple step drop casting procedure, a thermal treatment is included after each cycle. This means that the total time of thermal treatment is also multiplied. A longer thermal treatment means that the average penetration depth of the Mo precursor should increase, leading to a more homogeneous distribution of Mo within the hematite nanorods. For the same reason the accumulation of Mo on the surface should diminish. These changes in the Mo ditribution within the hematite samples would explain the slight differences found in the photocurrent enhancement of electrodes with the same Mo content prepared by each method. In addition, in the case of Figure 5 (one-step modification), the appearance of a second performance maximum is evident. This behavior can be explained on the basis of the dual role of Mo mentioned above. We may tentatively ascribe the second maximum to achieving an effective passivation of surface states as the amount of Mo introduced on the surface is large enough. Such a passivating layer is probably composed of an iron-molybdenum oxide (such as ferric molybdate), which would explain the fact that the electrode is stable in alkaline solution in spite of the fact that the oxygenated Mo(VI) species are soluble under these conditions.

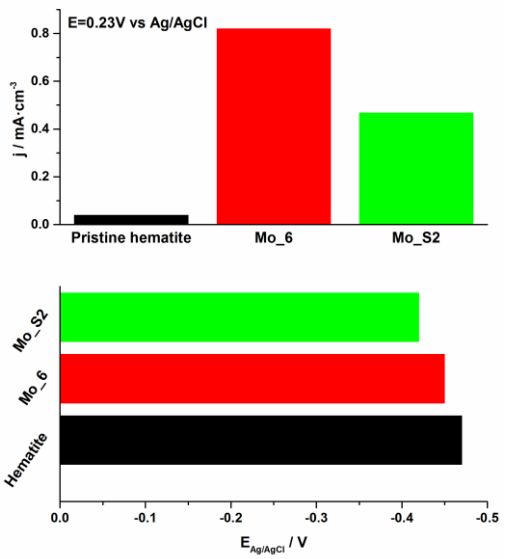

Figure 9. (a) Photocurrent density at 0.23 V and (b) photoonset potentials for the different hematite electrodes, obtained under illumination conditions of 350 mW·cm^{-2} (λ>350 nm) in N_2-purged aqueous 1M NaOH.

It is worth noting that our work on impregnation (drop casting) leads to conclusions similar to those advanced by McFarland *et al.* by using electrochemical co-deposition[25]. However, in the case of these authors, the co-deposition of Mo yields larger particles without a well-defined shape and a dense structure, while in our case the incorporation of Mo in the hematite nanorods (by either single- or multiple-step drop casting) does not trigger significant changes in structure and morphology. Regarding photoactivity, McFarland *et al.* found an improvement of 3x for 15%-Mo hematite co-deposited at 0.2V vs Ag/AgCl, compared to 43x and 26x in the cases of the Mo_6 and Mo_S2 electrodes obtained here (8.10 nmol Mo·cm^{-2} and 0.54 nmol Mo·cm^{-2} respectively).

Conclusions

Effective modification of hematite nanorod electrodes can be achieved by impregnation (drop casting) with aqueous solutions of a Mo precursor (ammonium heptamolybdate). One advantage of this modification method is that the morphology of the electrode is largely preserved and that the total amount of Mo introduced into hematite is quantitatively known. In fact, the amount of Mo is controlled through the concentration of the precursor solution or by repeating the drop casting procedure a number of times. The modification with Mo has effects on both the dark response of the electrodes and their photoactivity. In the first case, a clear increase of the voltammetric accumulation capacitance region is observed. In the second, a dramatic improvement of the photocurrent is achieved. In fact, for a hematite electrode modified with the addition of 8.10 nmol Mo·cm^{-2} (*Mo_6*), a 43-fold photocurrent multiplication has been achieved.

Several experimental results, including the shape of the photoactivity vs. Mo loading curves, strongly suggest that Mo has a double role in the modification of the hematite electrode response. On the one hand, it would increase the conductivity of hematite as a result of an increment of the majority carrier concentration. On the other, surface Mo species would act as a passivating agent, blocking surface states associated with the valence band. Probably, the electrode outermost layer is constituted by an iron molybdenum oxide (such as ferric molybdate) which would stabilize Mo(VI) surface species and thus the modified electrodes in contact with an alkaline solution.

Admittedly the incorporation of Mo into the hematite electrode triggers a shift of the photocurrent onset toward positive potentials. In this respect, future studies should focus on solving this limitation as well as on increasing photoactivity. Co-doping could be a very promising approach to solve the issues of hematite by judiciously choosing the combinations of different dopants and their concentrations. It is particularly interesting to combine cationic and anionic dopants, as this strategy could provide a way to separately affect both charge carriers. Studies along these lines are underway in our laboratory.

Experimental Section

Synthesis of (110) oriented hematite nanorods

The employed methodology is based on the work of Vayssieres and co-workers, who proposed a synthetic route to prepare (110) oriented α-Fe_2O_3 nanorod arrays by controlled growth from aqueous solution. It consists of a chemical bath deposition followed by a thermal treatment [43–45]. All solutions were prepared with deionized water with resistivity higher than 15 MΩ·cm^{-1}. The experimental procedure consists of adding 80 mL of an aqueous solution containing 0.15 mol·L^{-1} ferric chloride ($FeCl_3·6H_2O$, Sigma-Aldrich, 99%) and 1 mol·L^{-1} sodium nitrate ($NaNO_3$, Panreac, 99%) into a regular stopped flask with fluorine tin oxide (FTO) glass substrates almost vertically supported on the flask wall. The flask is then heated in a regular oven at 100ºC for 6 h. Afterward, the resulting thin films are thoroughly washed with water to remove any residues. A heat treatment in air at 600ºC for 1 h was applied to obtain hematite thin films with a nanorod-based morphology. The as-prepared hematite electrodes were transparent, with a homogeneous red coloration.

Modification with Mo by drop casting

Once the hematite nanorod thin film is prepared, a drop of the Mo precursor aqueous solution is applied on it, ensuring that the hematite thin film was fully covered. The employed precursor is ammonium heptamolybdate tetrahydrate ($(NH_4)_6Mo_7O_{24}·4H_2O$, Fluka, 99%). By varying the concentration of the Mo precursor solution, different quantities of Mo were deposited. We express the deposited amount in terms of nmol Mo·cm^{-2} (of geometric electrode surface area). A straightforward nomenclature (shown in Table 1) has been used throughout the text (Mo_X samples). Immediately after applying the drop casting procedure, the electrodes were dried overnight at 100ºC followed by a heat treatment at 450ºC for 30 min.

A second procedure closely related to the first one was also studied. In this case, a fixed amount of Mo (0.54 nmol Mo·cm^{-2}) was added stepwise until attaining the same amounts used in the preparation of Mo_X samples. After each addition, a mild heat treatment (450ºC, 30 minutes) was performed, leading to Mo_SX samples.

Table 1. Nomenclature employed for the different Mo-doped hematite electrodes. The character *S* means that Mo-modification has been achieved by the application of several cycles of drop-casting+thermal treatment. The concentration of the Mo precursor, the number of drops and the final Mo loading on the electrode are given. The volume of a droplet is of 50μL.

Nomenclature		[$H_{24}Mo_7N_6O_{24}$] / μM	Number of drops		nmoles of Mo per cm^2
Mo_1	**Mo_S1**	8.10	1	1	0.54
Mo_2	**Mo_S2**	24.3	1	3	1.62
Mo_3	**Mo_S3**	40.4	1	5	2.70
Mo_4	**Mo_S4**	64.8	1	8	4.32
Mo_5	**Mo_S5**	121.4	1	10	5.40
Mo_6		182.13	1		8.10
Mo_7		242.9	1		10.80
Mo_8		330.0	1		13.50

Sample characterization

The crystal structure of hematite was identified by X-ray diffraction (Bruker D8-Advance, using Cu Ka radiation) with the rotatory anode operating at 40 kV and 40 mA in the 2Θ range from 20º to 70º with a step scan of 1º·min^{-1}.

SEM micrographs were recorded with a Field Emission Scanning Electron Microscope, FE-SEM (Zeiss Merlin VP Compact), equipped with an energy dispersive X-ray spectrometer (EDS), (Bruker Quantax 400). TEM micrographs were obtained with a Transmission Electron Microscope JEOL (model JEM-2010) equipped with an X-ray detector (OXFORD INCA Energy TEM 100) for microanalysis (EDS).

X-ray photoelectron spectroscopy (XPS) was used for compositional analysis and for characterizing the iron and molybdenum oxidation states (K-Alpha Thermo-Scientific).

(Photo)electrochemical characterization

(Photo)electrochemical measurements were carried out in a standard three-electrode two-compartment electrochemical cell using the hematite films (or Mo-modified hematite films) as working electrodes (1.2 cm^2 geometric area) and an Ag/AgCl/KCl (sat) electrode as a reference electrode (to which all the potentials are referred unless otherwise stated). A platinum wire was used as a counter electrode. The working electrolyte was a 1 mol·L^{-1} NaOH (Panreac, 98%) solution. A scanning potentiostat (Potenciostat/Galvanostat AUTOLAB PGSTAT30) was used to record voltammograms in the dark and under illumination at a scan rate of 50 mV·s^{-1} (cyclic voltammetry) or 10 mV·s^{-1} (linear sweep voltammetry). In addition to voltammetry, Mott-Schottky plots, and electrochemical impedance spectra were measured with this instrument. The solution was purged with N_2 before and during the experiments. A 1000 W ozone-free xenon arc lamp (ORIEL Newport) was used for illumination. The lamp radiation was filtered through a water filter and a cut filter (Newport FSR-KG3 λ≥350 nm). The hematite electrodes were illuminated from the electrolyte side. The incident light intensity was measured with a thermopile (Thorlabs PM100D) (power density around 350 mW·cm^{-2}).

Acknowledgements

We are grateful to the Spanish MINECO for financial support through projects MAT2012-37676 and MAT2015-71727-R both supported with FEDER funds. A. C. wants to thank the Vicepresidency of Research, Development and Innovation of University of Alicante for financial support through an initiation research grant. D. C. is also grateful to MINECO for the award of an FPI grant.

Keywords: hematite; doping; molybdenum; photoelectrochemistry; water splitting

Supporting information (SI) available: Additional experimental details, morphological characterization, photoelectrochemical plots, stability test, XPS spectra and Mott-Schottky plots.

[1] G. Wang, Y. Ling, H. Wang, L. Xihong, Y. Li, *J. Photochem. Photobiol. C Photochem. Rev.* **2014**, *18*, 35–51.

[2] T. Bak, J. Nowotny, M. Rekas, C. Sorrell, *Int. J. Hydrogen Energy* **2002**, *27*, 991–1022.

[3] P. Bornoz, F. F. Abdi, S. D. Tilley, B. Dam, R. Van De Krol, M. Grätzel, K. Sivula, *J. Phys. Chem. C* **2014**, *118*, 16959–16966.

[4] M. S. Prévot, K. Sivula, *J. Phys. Chem. C* **2013**, *117*, 17879–17893.

[5] A. Fujishima, K. Honda, *Nature* **1972**, *238*, 37–38.

[6] D. Jing, L. Guo, L. Zhao, X. Zhang, H. Liu, M. Li, S. Shen, G. Liu, X. Hu, X. Zhang, *Int. J. Hydrogen Energy* **2010**, *35*, 7087–7097.

[7] T. Berger, D. Monllor-Satoca, M. Jankulovska, T. Lana-Villarreal, R. Gómez, *ChemPhysChem* **2012**, *13*, 2824–2875.

[8] B. Klahr, S. Gimenez, F. Fabregat-Santiago, J. Bisquert, T. W. Hamann, *Energy Environ. Sci.* **2012**, *5*, 7626–7636.

[9] M. A. Butler, *J. Appl. Phys.* **1977**, *48*, 1914–1920.

[10] C. Lin, D. Mersch, D. A. Jefferson, E. Reisner, *Chem. Sci.* **2014**, *5*, 4906–4913.

[11] X. Huang, Q. Shen, J. Liu, N. Yang, G. Zhao, *Energy Environ. Sci.* **2016**, *9*, 3161–3171.

[12] J. Fan, Z. Chen, H. Shi, G. Zhao, *Chem. Commun.* **2016**, *52*, 4290–4293.

[13] K. Sivula, F. Le Formal, M. Grätzel, *ChemSusChem* **2011**, *4*, 432–449.

[14] G. Gurudayal, S. Y. Chiam, M. H. Kumar, P. S. Bassi, H. L. Seng, J. Barber, L. H. Wong, *ACS Appl. Mater. Interfaces* **2014**, *6*, 5852–5859.

[15] J. J. Deng, A. W. Pu, M. Li, J. Gao, H. Zhang, J. Zhong, X. H. Sun, A. T. H. Nanostructures, *Int. Conf. Nanotechnol.*, **2014**,75–78.

[16] N. Iordanova, M. Dupuis, K. M. Rosso, *J. Chem. Phys.* **2005**, *122*, 144305–10.

[17] T. Nakau, *J. Phys. Soc. Japan* **1960**, *15*, 727.

[18] K. M. Rosso, D. M. A. Smith, M. Dupuis, *J. Chem. Phys.* **2003**, *118*, 6455–6466.

[19] N. J. Cherepy, D. B. Liston, J. A. Lovejoy, H. Deng, J. Z. Zhang, *J. Phys. Chem. B* **1998**, *102*, 770–776.

[20] A. G. Joly, J. R. Williams, S. A. Chambers, G. Xiong, W. P. Hess, D. M. Laman, *J. Appl. Phys.* **2006**, *99*, 53521–6.

[21] S. R. Pendlebury, M. Barroso, A. J. Cowan, K. Sivula, J. Tang, M. Grätzel, D. Klug, J. R. Durrant, *Chem. Commun. (Camb).* **2011**, *47*, 716–718.

[22] S. Shen, *J. Mater. Res.* **2013**, *29*, 1–18.

[23] M. J. Katz, S. C. Riha, N. C. Jeong, A. B. F. Martinson, O. K. Farha, J. T. Hupp, *Coord. Chem. Rev.* **2012**, *256*, 2521–2529.

[24] G. Wang, Y. Ling, D. a Wheeler, K. E. N. George, K. Horsley, C. Heske, J. Z. Zhang, Y. Li, *Nano Lett.* **2011**, *11*, 3503–3509.

[25] A. Kleiman-Shwarsctein, Y. S. Hu, A. J. Forman, G. D. Stucky, E. W. McFarland, *J. Phys. Chem. C* **2008**, *112*, 15900–15907.

[26] X. Zhang, H. Li, S. Wang, F. R. F. Fan, A. J. Bard, *J. Phys. Chem. C* **2014**, *118*, 16842–16850.

[27] R. Shinar, J. H. Kennedy, *Sol. Energy Mater.* **1982**, *6*, 323–335.

[28] P. Kumar, P. Sharma, R. Shrivastav, S. Dass, V. R. Satsangi, *Int. J. Hydrogen Energy* **2011**, *36*, 2777–2784.

[29] Y. Ling, Y. Li, *Part. Part. Syst. Charact.* **2014**, *31*, 1113–1121.

[30] H. S. Oliveira, L. D. Almeida, V. A. A. De Freitas, F. C. C. Moura, P. P. Souza, L. C. A. Oliveira, *Catal. Today* **2015**, *240*, 176–181.

[31] J. Liu, Y. Y. Cai, Z. F. Tian, G. S. Ruan, Y. X. Ye, C. H. Liang, G. S. Shao, *Nano Energy* **2014**, *9*, 282–290.

[32] A. Gajović, A. M. T. Silva, R. a. Segundo, S. Šturm, B. Jančar, M. Čeh, *Appl. Catal. B Environ.* **2011**, *103*, 351–361.

[33] C. Brookes, P. P. Wells, G. Cibin, N. Dimitratos, W. Jones, D. J. Morgan, M. Bowker, *ACS Catal.* **2014**, *4*, 243–250.

[34] J. C. Launay, G. Horowitz, *J. Cryst. Growth* **1982**, *57*, 118–124.

[35] S. Park, H. Jin, C. Woo, H. Jo, S. Sik, S. Won, H. Kee, S. Lee, D. Kim, K. Sun, *Int. J. Hydrogen Energy* **2014**, *39*, 16459–16467.

[36] J. Liu, C. Liang, G. Xu, Z. Tian, G. Shao, L. Zhang, *Nano Energy* **2013**, *2*, 328–336.

[37] H. Zhao, W. Fu, H. Yang, Y. Xu, W. Zhao, Y. Zhang, H. Chen, Q. Jing, X. Qi, J. Cao, et al., *Appl. Surf. Sci.* **2011**, *257*, 8778–8783.

[38] M. Tallarida, C. Das, D. Cibrev, K. Kukli, A. Tamm, M. Ritala, T. Lana-Villarreal, R. Gómez, M. Leskelä, D. Schmeisser, *J. Phys. Chem. Lett.* **2014**, *5*, 3582–3587.

[39] H. Pan, X. Meng, J. Cai, S. Li, G. Qin, *RSC Adv.* **2015**, *5*, 19353–19361.

[40] B. V. R. Chowdari, K. L. Tan, W. T. Chia, R. Gopalakrishnan, *J. Non. Cryst. Solids* **1990**, *119*, 95–102.

[41] M. Anwar, C. A. Hogarth, R. Bulpett, *J. Mater. Sci.* **1989**, *24*, 3087–3090.

[42] S. Chatman, C. I. Pearce, K. M. Rosso, *Chem. Mater.* **2015**, *27*, 1665–1673.

[43] T. Lindgren, H. Wang, N. Beermann, L. Vayssieres, A. Hagfeldt, S.-E. Lindquist, *Sol. Energy Mater. Sol. Cells* **2002**, *71*, 231–243.

[44] N. Beermann, L. Vayssieres, S.-E. Lindquist, A. Hagfeldt, *J. Electrochem. Soc.* **2000**, *147*, 2456–2461.

[45] L. Vayssieres, N. Beermann, S. E. Lindquist, a. Hagfeldt, *Chem. Mater.* **2001**, *13*, 233–235.

ARTICLE

Modification of hematite nanorod electrodes with molybdenum by an impregnation method leads to a drastic enhancement of their photoactivity.

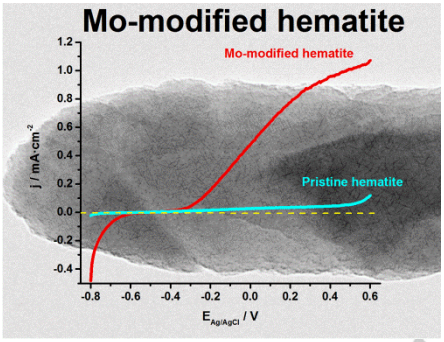

*Ainhoa Cots, Dejan Cibrev, Pedro Bonete, Roberto Gómez**

Page No. – Page No.

Title: Hematite Nanorod Electrodes Modified with Molybdenum: Photoelectrochemical Studies.